


Article

Preparation and Tribological Behaviors of Antigorite and Wollastonite Mineral Dual-Phase-Reinforced Polytetrafluoroethylene Matrix Composites

Chen Wang^{1,2}, Helong Yu^{2,*}, Yanli Yin², Xinyuan Zhou², Hongmei Wang^{2,3}, Zhanyong Song³, Shen Wang^{1,2}, Zhe Yang^{2,4} and Zhimin Bai^{1,*}

¹ School of Materials Science and Engineering, China University of Geosciences, Beijing 100083, China; 2103210003@email.cugb.edu.cn (C.W.); wangshen3296@163.com (S.W.)

² National Key Lab for Remanufacturing, Army Academy of Armored Forces, Beijing 100072, China; yinyl2009@126.com (Y.Y.); zxyuan1202@163.com (X.Z.); whmspj@163.com (H.W.); 15806726444@163.com (Z.Y.)

³ Department of Support and Remanufacture Engineering, Army Academy of Armored Forces, Beijing 100072, China; stranger303@163.com

⁴ School of Printing, Packaging and Digital Media, Xi'an University of Technology, Xi'an 710048, China

* Correspondence: helong.yu@163.com (H.Y.); zhimibai@cugb.edu.cn (Z.B.)

Abstract: Research on polymer matrix composites with excellent tribological properties has received increasing attention in recent years. In this study, antigorite and wollastonite mineral dual-phase-reinforced polytetrafluoroethylene (PTFE) matrix composites were prepared by filling PTFE with mineral powders using ball-milling, cold-pressing, and pressureless sintering methods. The phase structure, microstructure, chemical composition, Shore hardness, and tribological behavior of the composites rubbed against steel balls under dry friction conditions were investigated. The results show that the composites have a dense structure and uniform distribution of mineral phases, with a Shore hardness of 62–68.8, an increase of 18.7–23.7% compared to pure PTFE. Compared with the addition of mono antigorite or wollastonite, the composites prepared by simultaneously filling the two minerals exhibited excellent tribological properties. The average friction coefficient and wear volume of the (10Atg + 20Wl)/PTFE composites were reduced by 44.2% and 71.4%, respectively, compared to those of pure PTFE. A dense and continuous tribofilm composed mainly of SiO₂, MgSiO₃, Mg₂SiO₄, MgO, CaO, CaMg(SiO₃)₂, and CaF₂ was formed on the worn surfaces of both the dual-phase-reinforced PTFE matrix composites and counterpart steel balls during the friction process. The reduction in friction and wear is attributed to the reinforcement effect of the minerals on the PTFE matrix as well as the complex physical and chemical reactions at the friction interface stimulated by the synergistic effects between the two minerals. The addition of wollastonite reduced the phase transition temperature of antigorite, promoting more tribochemical reaction products with good abrasion resistance and friction-reducing properties, which contributed to the excellent tribological behavior of the composites.

Keywords: antigorite; wollastonite; polytetrafluoroethylene; tribological behavior; tribofilm



Citation: Wang, C.; Yu, H.; Yin, Y.; Zhou, X.; Wang, H.; Song, Z.; Wang, S.; Yang, Z.; Bai, Z. Preparation and Tribological Behaviors of Antigorite and Wollastonite Mineral Dual-Phase-Reinforced Polytetrafluoroethylene Matrix Composites. *Lubricants* **2024**, *12*, 74. <https://doi.org/10.3390/lubricants12030074>

Received: 18 January 2024

Revised: 11 February 2024

Accepted: 21 February 2024

Published: 26 February 2024



Copyright: © 2024 by the authors. Licensee MDPI, Basel, Switzerland. This article is an open access article distributed under the terms and conditions of the Creative Commons Attribution (CC BY) license (<https://creativecommons.org/licenses/by/4.0/>).

1. Introduction

Polytetrafluoroethylene (PTFE), a fluorocarbon compound with a linear symmetric structure, has been widely used as an engineering and solid lubricating material because of its good self-lubricating ability, thermal stability, corrosion resistance, and machinability [1]. However, the PTFE molecular bond structure exhibits unique slip and creep characteristics during crystallization, resulting in poor wear resistance, which limits its applications [2,3]. Therefore, modification treatments, including surface, blending, and filling modifications, are necessary to improve the tribological properties of PTFE [4–6]. Among these, filling modification has been the focus of current research by introducing reinforced fibers (glass

or carbon fibers) and nanoparticles (metals and their oxides/sulfides and carbon materials) to prepare PTFE-based composites, which have advantages such as low material shrinkage, high stiffness and strength, and good comprehensive performances [7–9].

Phyllosilicate powders have a large specific surface area, and their unique layered structure and crystallographic characteristics endow them with excellent adsorptivity, expansibility, and ion exchange properties [10]. With the advantages of good self-lubrication, catalytic performance, and high tribochemical reactivity with metal surfaces, phyllosilicate minerals used as lubricating oil (grease) additives exhibit excellent anti-wear and friction-reducing performance [11]. The addition of minerals can not only significantly reduce the friction coefficient and wear of metals but also improve the mechanical properties of worn metal surfaces by forming a hard self-healing film through dehydration reactions, group recombination, and tribochemical reactions during the friction process [12]. Related research in tribology and intelligent self-healing materials has always been a hot topic.

Based on research on lubricant additives, studies on improving the mechanical and tribological properties of PTFE using phyllosilicate powders, such as serpentine, attapulgite, and sepiolite, as fillers have attracted considerable attention in recent years owing to their ability to intercalate monomers or polymer molecules [13,14]. This is an effective approach to avoid organic modification of mineral powders and solve the problem of powder additive dispersion stability in lubricants by introducing phyllosilicate minerals into polymers to improve their tribological properties. Jia et al. [15] prepared serpentine/PTFE composites by filling serpentine powder into PTFE. The uniformly dispersed serpentine particles effectively prevented the severe adhesive wear of PTFE, and a relatively stable and low friction coefficient was achieved owing to the existence of the serpentine particulates, which acted as effective barriers for the large-scale adhesive wear of the PTFE matrix. Zhao et al. [16] filled ultrahigh-molecular-weight polyethylene (UHMWPE) with attapulgite powder and prepared composites with good thermal stability and denser microstructures. The coefficient of friction was reduced by 29%, and the specific wear rate was decreased by 42% with the addition of 1 wt.% attapulgite. Lai et al. [17] prepared PTFE-based composites by filling attapulgite into PTFE, which showed a wear rate several orders of magnitude lower than that of pure PTFE. Moreover, it has been demonstrated that the simultaneous introduction of layered silicates with other inorganic powders into polymeric materials can produce a synergistic effect and further improve the tribological properties of the composites. Tarasova et al. [18] found that the filling of kaolin and magnesium spinel into PTFE increased its wear resistance by three orders of magnitude. In addition, recent research by Liu et al. [19] showed that wollastonite minerals can significantly improve the tribological properties of polymers containing 70 wt.% wollastonite composites of the abrasion resistance, as the worn surface produces only a slight furrow. Wu et al. [20] prepared (attapulgite + wollastonite)/PTFE composites by combining mechanical stirring with a cold-press sintering process, which showed a significant increase in hardness compared with pure PTFE, a slight raise in friction coefficient, but a remarkable reduction in wear rate.

Considering the significant efficacy of mono antigorite or wollastonite minerals in improving the tribological properties of polymeric materials and the possible synergistic effect of their simultaneous addition, this study introduces antigorite and wollastonite powders into PTFE as fillers, and prepared antigorite/wollastonite mineral dual-phase-reinforced PTFE matrix composites with different compositions by combining cold-press molding with a pressureless sintering method. The phase structure, microstructure, chemical composition, Shore hardness, and tribological behavior of the composites were systematically investigated. The mechanism of the friction and wear improvement of PTFE caused by antigorite and wollastonite is discussed based on worn surface analysis. The present work is expected to support the development of mineral materials such as antigorite and wollastonite as functional fillers for polymer engineering materials, such as polytetrafluoroethylene.

2. Experimental Procedures

2.1. Materials

Figure 1 shows the morphologies and particle size distributions of the raw powders. Antigorite (Atg), with a median diameter (D50) of 4.510 μm , was extracted from the natural serpentine mineral in Anshan, Liaoning Province, China, and powdered raw materials with lamellar structures were obtained using a jaw crusher combined with a vibratory mill refining process. To improve the dispersion stability of antigorite minerals in the polymer matrix and increase their tribochemical reactivity during friction, the mineral was mechanically activated using a ball-milling method before mixing it with other raw powders [20]. The raw materials are activated using a planetary ball mill, and the ball-milling jars are made of PTFE ball-milling jars in an atmospheric atmosphere. During ball milling, the mass ratio of zirconia balls ($\phi 6 \text{ mm}:\phi 1 \text{ mm} = 4:6$) and antigorite powder to distilled water was 10:1:1.5, the ball mill speed was 300 rpm, and the duration was 10 h. After ball milling, the treated mineral was filtered, dried at 120 $^{\circ}\text{C}$, and ground to obtain activated antigorite powder. After the activation treatment, the size of the antigorite particles significantly decreased, and the median particle size (D50) of the powder decreased from 4.510 μm to 0.786 μm . Wollastonite (Wl), with a median diameter (D50) of 3.852 μm , was provided by Dalian Global Mineral Co., Ltd. (Dalian, China). Polytetrafluoroethylene (PTFE) powder with a diameter of approximately 2 μm was purchased from Shandong Dongyue Company (Zibo, China).

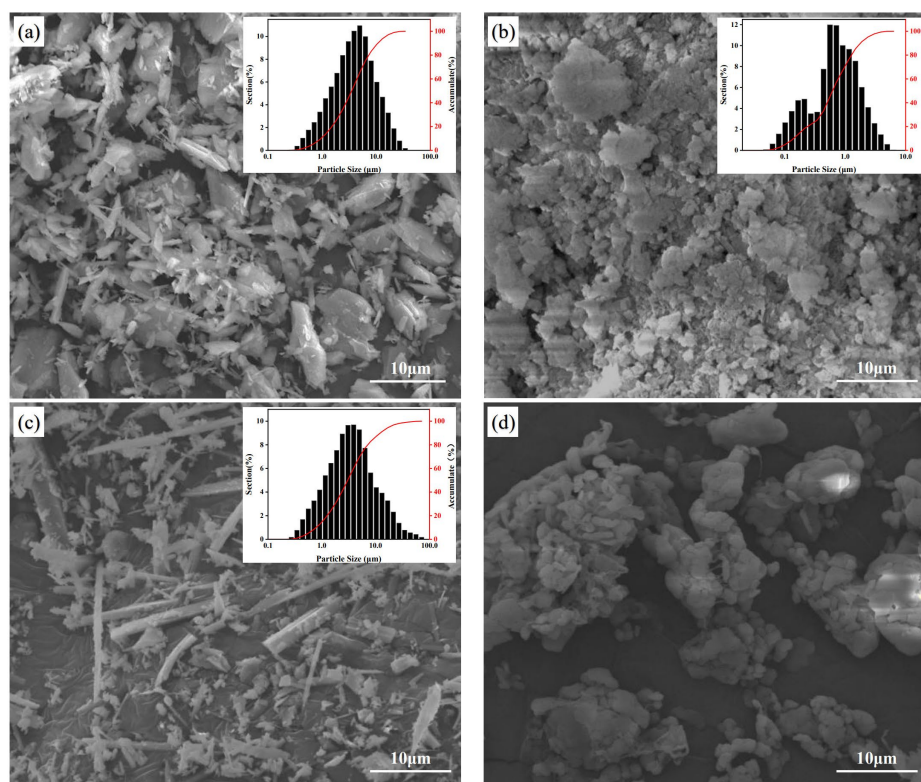


Figure 1. SEM images and particle size distribution of (a) untreated antigorite, (b) ball-milled antigorite, (c) wollastonite, and (d) PTFE raw powders.

2.2. Preparation of PTFE Matrix Composites

Figure 2 shows a schematic of the preparation process of the PTFE matrix composites. The powders of PTFE, wollastonite, and activated antigorite mineral were dried in a vacuum drying oven at 120 $^{\circ}\text{C}$ for 4 h to remove surface-adsorbed water. Subsequently, the raw materials were mixed using a ball mill (300 r/h, 5 h) according to the compositions listed in Table 1. The samples to be sintered, with dimensions $\phi 20 \text{ mm} \times 3 \text{ mm}$, were

obtained by cold-press molding of the mixed raw powders, uniform pressure to 60 Mpa, holding pressure for 30 min.

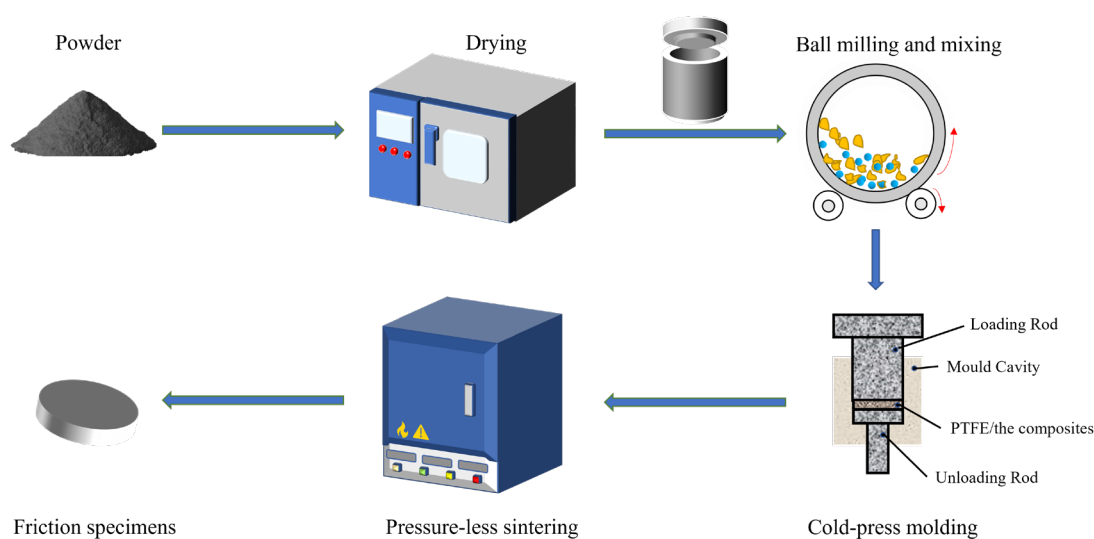


Figure 2. Schematic diagram of the preparation process for PTFE matrix composites.

Table 1. Compositions of the raw powders to be sintered.

Sample No.	Raw Powders, wt. %		
	PTFE	Atg	WI
Pure PTFE	100	0	0
10Atg/PTFE	90	10	0
10WI/PTFE	90	0	10
(10Atg + 10WI)/PTFE	80	10	10
(10Atg + 20WI)/PTFE	70	10	20
(10Atg + 30WI)/PTFE	60	10	30
(15Atg + 20WI)/PTFE	65	15	30
(20Atg + 20WI)/PTFE	60	20	30

PTFE matrix composites with different compositions were prepared by pressureless sintering according to the heat treatment process curve shown in Figure 3. Sintering was performed using a muffle furnace at standard atmospheric pressure. Starting from room temperature, the sample was heated to 327 °C at a rate of 1 °C/min and held for 120 min; subsequently, the sample was heated to 375 °C at a rate of 1 °C/min and held for 90 min; after that, the sample was naturally cooled to room temperature in the sintering furnace. Based on the compositions of the raw powders listed in Table 1, the composite samples are referred to as 10Atg/PTFE, 10WI/PTFE, (10Atg + 10WI)/PTFE, (10Atg + 20WI)/PTFE, (10Atg + 30WI)/PTFE, (15Atg + 20WI)/PTFE, and (20Atg + 20WI)/PTFE, respectively.

2.3. Characterization Method

A Bruker D8 Advance X-ray diffractometer (XRD) (BRUKER, Karlsruhe, Germany) was used to determine the phase structures of the composites. The scanning speed was 5°/min, and the 2θ range was 5–80° during the test. The X-ray generator (BRUKER, Karlsruhe, Germany) is a ceramic sealed tube, and the anode target is a copper target, corresponding to an X-ray wavelength of 0.154056 nm. Fourier transform infrared spectroscopy (FT-IR, Nicolet 6700) (Thermo Nicolet Corporation, Guangzhou, China) was used to determine the functional groups of the composites. The spectra were recorded 32 times scanning each measure, in the range from 4000 cm⁻¹ to 400 cm⁻¹ with resolution of 4 cm⁻¹, and a simultaneous thermal analyzer (SAT, NETZSCH STA 449C) (NETZSCH, Bavaria,

Germany) was used to perform thermodynamic analysis of the mixed raw powders. Nitrogen was used as a protective gas at a heating rate of 10 °C/min. A Shore hardness tester (LX-D) (Shanghai, China) was used to measure the hardness of the composites. Five test points were randomly selected for each sample, and the average value was taken as the measurement result.

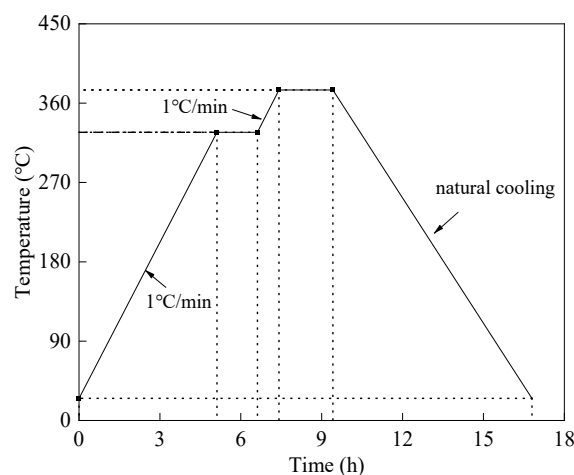


Figure 3. Temperature curve for pressureless sintering of PTFE matrix composite.

An Optimal SRV-IV ball-on-disc friction and wear tester (optimol fats & oils, Ulm, Germany) was used to evaluate the tribological properties of the composites. The upper reciprocating specimen was a GCr15 steel ball (HRC59-61, ϕ 10 mm) with a sliding stroke of 1 mm, duration of 30 min, reciprocating frequency of 20 Hz, and load of 15 N. Testing was performed at room temperature 25 °C. The composites and GCr15 steel balls were ultrasonically cleaned at 450 W for 10 min prior to testing. The friction coefficient was automatically recorded in real time using the tester.

After the wear test, an Olympus LEXT OLS4000 3D laser (Olympus, Tokyo, Japan) confocal microscope was used to measure the 3D morphology, surface roughness, and wear volume of the worn composite surfaces. The morphologies and elemental compositions of the worn surfaces of both the composites and paired steel balls were examined using FESEM (Field Emission Scanning Electron Microscopy) and EDS (Energy Dispersive Spectrometer). The chemical state of the main elements on the worn steel ball surface was determined by a Thermo Fisher ESCLAB 250Xi multifunctional X-ray photoelectron spectrometer (XPS) (Thermo Fisher, Waltham, MA, USA), with a monochromatic Al target as the emission source, an energy resolution of ± 0.2 eV, a pass energy of 29.4 eV, and a standard carbon contamination peak (C1s at 284.8 eV) as the reference.

An FEI 3D quantum scanning electron microscope and focused ion beam (SEM/FIB) workstation (Thermo Fisher, Waltham, MA, USA) were used to prepare the cross-sectional specimen of the worn steel ball surface rubbing against the PTFE matrix composite for TEM analysis. The specimen was then analyzed using a Tecnai G2 F20 high-resolution transmission electron microscope (HRTEM) (Thermo Fisher, Waltham, MA, USA). Additionally, an Agilent G200 nanoindentation tester (Agilent, Santa Clara, CA, USA) was used to determine the nanomechanical properties of the worn steel surfaces in CSM mode. The maximum indentation depth was 2000 nm. A Poisson's ratio of 0.25 was used for the calculation of the elastic modulus.

3. Results and Discussion

3.1. Phase and Microstructure

Figure 4 shows the XRD patterns of composites with different compositions. Distinct PTFE, antigorite, and wollastonite diffraction peaks were identified in the XRD patterns of the composites. The intensity of X-ray diffraction peaks of the composites was signifi-

cantly reduced compared to that of the pure PTFE. This may be because the addition of mineral powder hinders the nucleation and crystallization of PTFE, leading to a decrease in the crystallinity of the composites [21]. During the polymer crystallization process, the polymer chain folds up and will form an orderly region with a certain degree of regularity. When mineral powder is added, the polymer chain polymerization process will receive obstruction, which reduces its crystallinity.

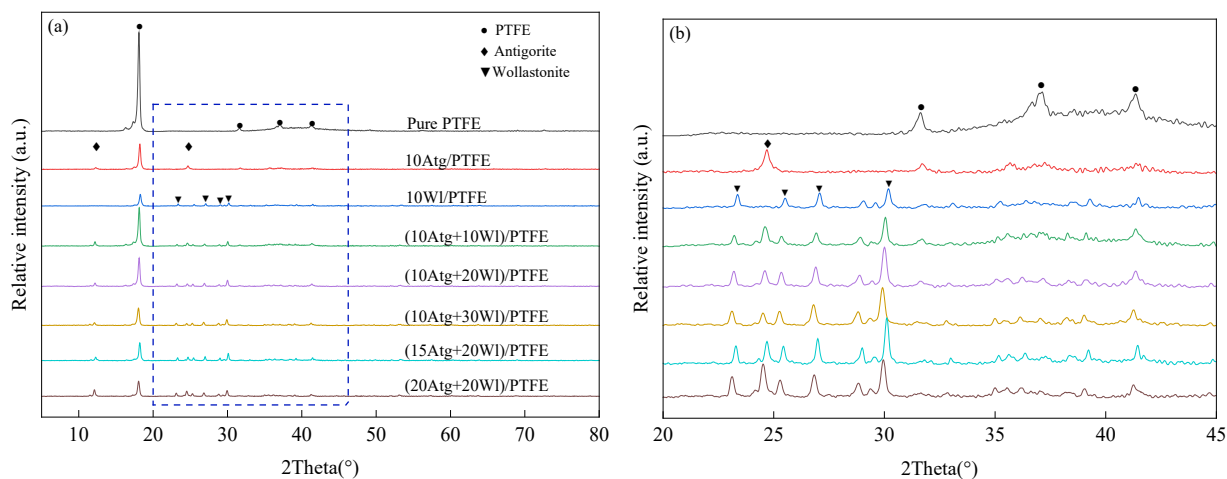


Figure 4. XRD patterns of PTFE and the composites with different compositions determined in (a) 2 θ range of 5–80° and (b) enlarged image of 20–45°.

Figure 5 shows the FT-IR spectra of composites with different compositions. The characteristic peaks of PTFE at 1201 cm^{-1} and 1143 cm^{-1} correspond to the symmetric stretching vibration absorption peaks and asymmetric stretching vibration absorption peaks of the C-F bond [22], respectively. For PTFE filled with antigorite, a hydroxyl stretching vibration peak (3680 cm^{-1}) and a hydroxyl bending vibration absorption peak (643 cm^{-1}) appeared, which connected the Si-O tetrahedron and Mg-O octahedron in the antigorite structure. Characteristic peaks reflecting the stretching vibration of Si-O bonds, bending vibration of Mg-O bonds, and bending vibration of Si-O bonds were observed at 1082 and 989 cm^{-1} , 593 cm^{-1} , and 442 cm^{-1} , respectively [23]. For PTFE filled with wollastonite, the characteristic peak reflected the asymmetric stretching vibration of Si-O-Si, and the absorption peak reflecting the symmetric stretching vibration appeared at 1008 cm^{-1} and 684 cm^{-1} , respectively. In addition, an absorption peak reflecting the symmetric stretching vibration of O-Si-O was observed at 961 cm^{-1} [24]. These results indicate that no new functional groups appeared during the introduction of antigorite and wollastonite powders into PTFE using the pressureless sintering method, indicating that no chemical reaction occurred between the raw powders.

The microstructural characterization of the (10Atg + 20Wl)/PTFE composites was analyzed as an example because of the similarity of the microstructures in all the mineral-containing composites. Figure 6 shows the SEM images and elemental distribution maps of the (10Atg + 20Wl)/PTFE composites. According to the distribution states of the characteristic elements Ca and Mg, which belong to the antigorite powder and wollastonite powder, respectively, it can be determined that antigorite and wollastonite are evenly dispersed in the PTFE matrix. Moreover, the mineral particles were tightly bonded to the PTFE matrix, and no obvious defects such as pores and cracks were observed in the composites.

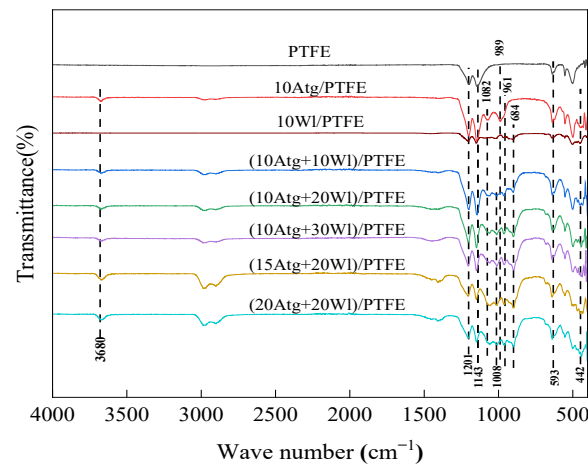


Figure 5. FTIR spectra of PTFE and the composites with different compositions.

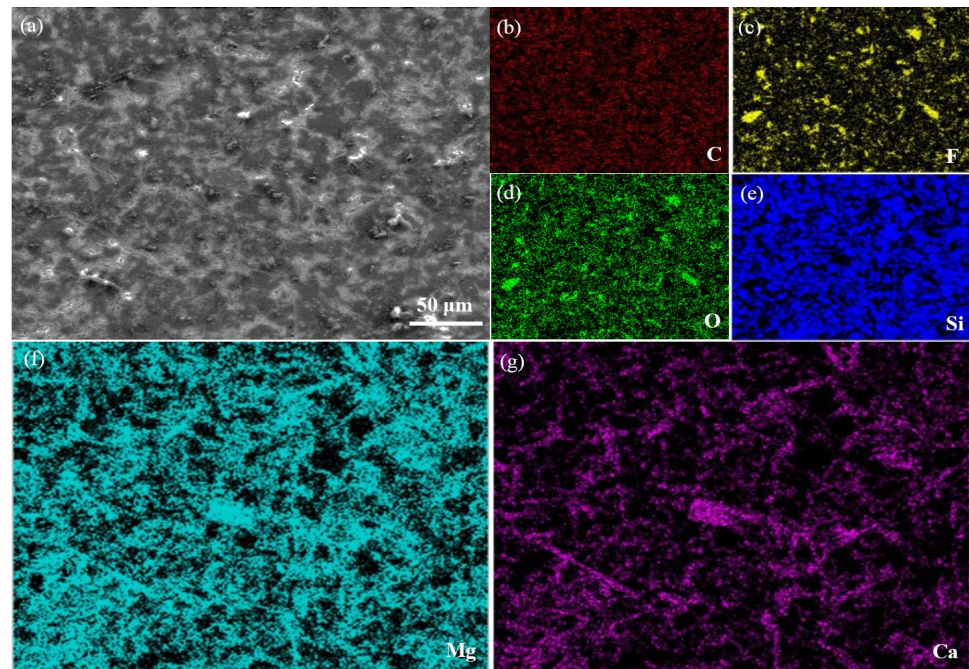


Figure 6. SEM images (a) and elemental distribution maps of (b) C, (c) F, (d) O, (e) Si, (f) Mg, and (g) Ca in the (10Atg + 20Wl)/PTFE composites.

3.2. Shore Hardness

Figure 7 shows the Shore hardness of the composites with different compositions. The Shore hardness of pure PTFE was approximately 55.6 HD. The Shore hardness of the composites improved owing to the filling of single-phase or multiphase mineral powders. In comparison, the hardness of the composites filled with wollastonite was superior to that filled with antigorite, and simultaneously filling antigorite and wollastonite into PTFE produced a better hardening effect than mono addition. The (10Atg + 30Wl)/PTFE sample exhibited the highest hardness, reaching 68.8 HD, which was 23.7% higher than that of the pure PTFE. The increase in composite hardness induced by the filling of the mineral powders may be related to two factors. Firstly, the Mohs hardness of the antigorite and wollastonite minerals reaches 2.5–4 and 4.5–5.5, respectively. Mineral powders have higher hardness than PTFE, which can reinforce the matrix to a certain extent. Secondly, the mineral powders uniformly dispersed in the matrix can restrict the movement of the polymer chains in PTFE during loading because of their higher stiffness, thereby improving the resistance of the composites to plastic deformation [25]. However, when the mineral

powders were overfilled, more interfaces and potential defects were generated within the composites, leading to a decrease in the hardness. Therefore, the Shore hardness of the PTFE matrix composites first increased and then decreased with an increase in the addition of antigorite and wollastonite.

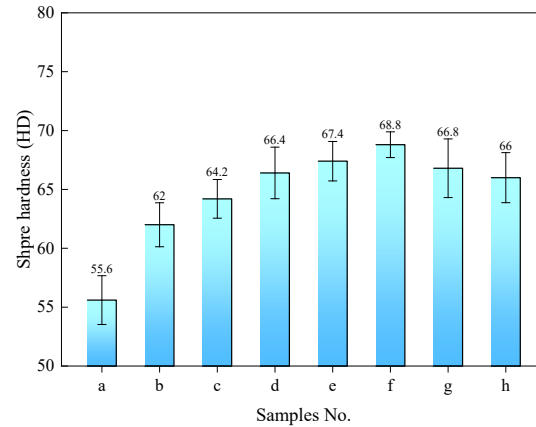


Figure 7. Shore hardness of (a) PTFE, (b) 10Atg/PTFE, (c) 10Wl/PTFE, (d) (10Atg + 10Wl)/PTFE, (e) (10Atg + 20Wl)/PTFE, (f) (10Atg + 30Wl)/PTFE, (g) (15Atg + 20Wl)/PTFE, and (h) (20Atg + 20Wl)/PTFE composites.

3.3. Friction and Wear Behaviors

Figure 8 shows the variation in the friction coefficient with time, average coefficient, and wear volume of PTFE and the composites under dry friction conditions when rubbing against GCr15 steel balls. The filling of mineral powders can significantly improve the wear resistance and friction reduction performance of PTFE, except for the ineffective effect of single-phase wollastonite minerals in reducing the friction coefficient. Compared with pure PTFE, the addition of a single-phase antigorite mineral had little effect on the friction coefficient reduction, but significantly reduced the time-variant fluctuation amplitude of the coefficient. The simultaneous filling of PTFE with dual-phase minerals produced better tribological properties than the mono-additive. The (10Atg + 20Wl)/PTFE composites showed the lowest friction coefficient and wear volume, with average friction coefficients and wear volumes of approximately 0.173 and $0.547 \times 10^8 \mu\text{m}^3$, respectively, which were approximately 44.2% and 71.4% lower than those of pure PTFE, respectively.

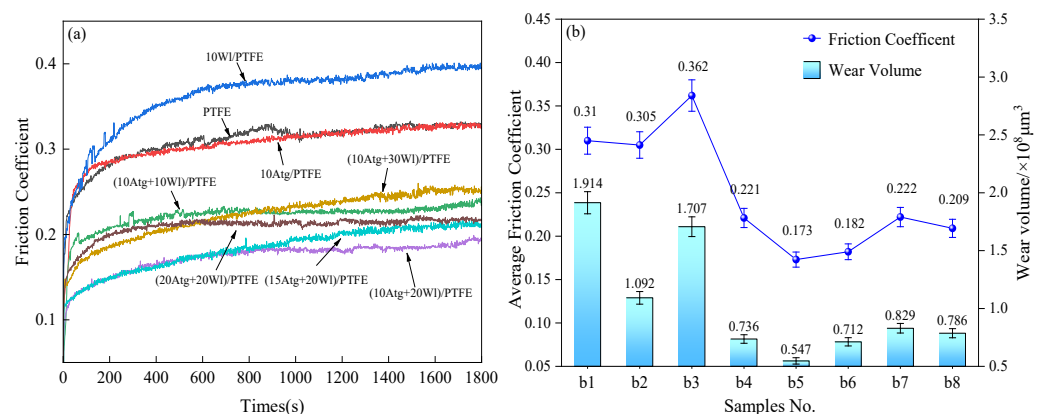


Figure 8. Variation in friction coefficient with time (a), wear volume, and average friction coefficient for (b1) PTFE, (b2) 10Atg/PTFE, (b3) 10Wl/PTFE, (b4) (10Atg + 10Wl)/PTFE, (b5) (10Atg + 20Wl)/PTFE, (b6) (10Atg + 30Wl)/PTFE, (b7) 15Atg + 20Wl)/PTFE, and (b8) (20Atg + 20Wl)/PTFE composites. (b) wear volume and average friction coefficient.

3.4. Worn Composites Surface Analysis

Figure 9 shows the 2D/3D morphologies and cross-sectional profile curves of the worn trace on the pure PTFE and the composites. Compared to pure PTFE, the worn trace dimensions of the 10Atg/PTFE composites were significantly reduced, and the surface roughness, Ra, decreased from 5.353 μm to 3.219 μm . The worn surface roughness of the 10Wl/PTFE composite was further reduced to Ra = 3.152 μm , although the reduction in wear volume was not significant. In contrast, the (10Atg + 20Wl)/PTFE composites exhibited a minimum wear volume and surface roughness Ra value of only 2.394 μm .

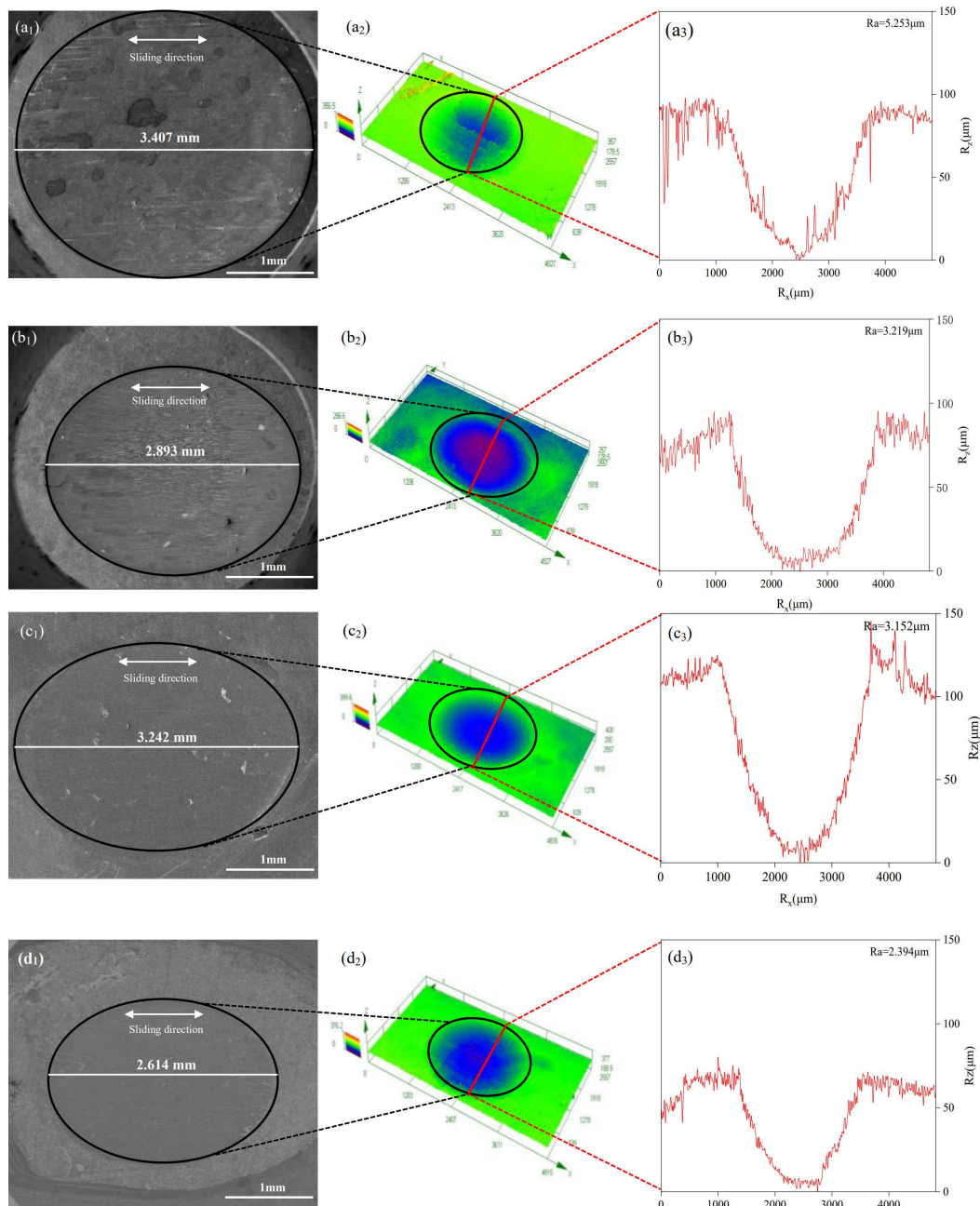


Figure 9. 2D/3D morphology and cross-sectional profile curve of the worn surface of (a₁–a₃) PTFE, (b₁–b₃) 10Atg/PTFE, (c₁–c₃) 10Wl/PTFE, and (d₁–d₃) (10Atg + 20Wl)/PTFE composites.

Figure 10 shows the SEM images and EDS patterns of the worn surfaces of pure PTFE and the composites. Several deep scratches parallel to the sliding direction, wear debris, material spalling, and local plastic deformations were observed on the worn PTFE surface,

indicating severe abrasive and adhesive wear. The wear of the 10Atg/PTFE composite was significantly reduced by the addition of antigorite powder to PTFE. The worn surface is relatively smooth, and only shallow scratches and a small amount of abrasive debris are observed. For the 10Wl/PTFE composites, the worn surface became smoother and flatter. The wear of the composites was further reduced by simultaneous addition of antigorite and wollastonite. Only a few microfine scratches are observed on the worn surfaces. The EDS analysis results indicated that the addition of antigorite and wollastonite resulted in the appearance of characteristic mineral elements, such as Si, Ca, Mg, and Al, on the worn surface, indicating that the addition of minerals is the main reason for the improvement in the wear resistance of the composites.

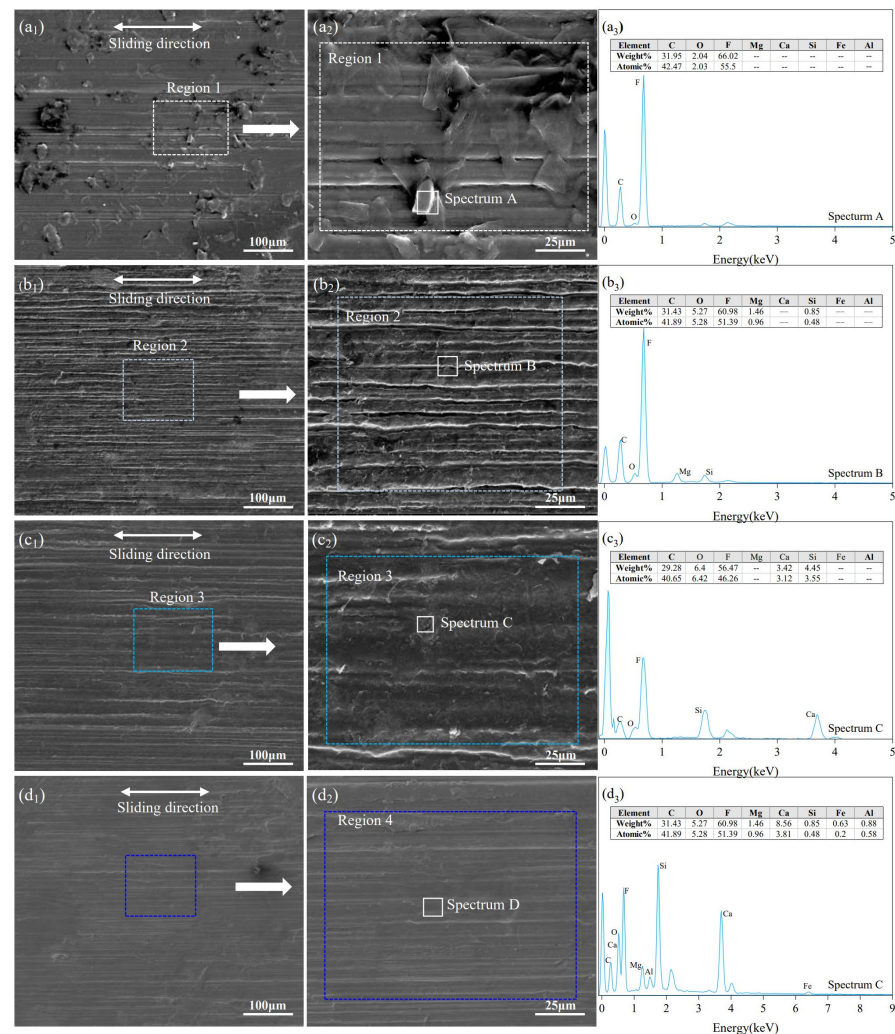


Figure 10. SEM images and EDS patterns of the worn surface of (a₁–a₃) PTFE, (b₁–b₃) 10Atg/PTFE, (c₁–c₃) 10Wl/PTFE, and (d₁–d₃) (10Atg + 20Wl)/PTFE composites.

Figure 11 shows the XPS spectra of the main elements on the unworn and worn surfaces of the (10Atg + 20Wl)/PTFE composite. For the unworn surface of (10Atg + 20Wl)/PTFE composites, the C1s spectrum can be fitted as two subpeaks located at 284.8 eV and 292.01 eV, corresponding to graphite and (C₂F₄)_n, respectively. The O1s spectrum can be fitted into subpeaks representing (Al/Mg)Si₄O₁₀(OH)₂·nH₂O (531.78 eV). The Mg1s spectrum indicated the presence of (Al/Mg)Si₄O₁₀(OH)₂·nH₂O at 1305.88 eV. The Si2p spectrum can be fitted into subpeaks of (Al/Mg)Si₄O₁₀(OH)₂·nH₂O at 101.67 eV, CaSiO₃ at 102.73 eV, and SiO₂ at 103.63 eV. The Ca2p spectrum indicated the presence of CaSiO₃ (347.19 eV) and CaO (351.16 eV). For the worn surface of the (10Atg + 20Wl)/PTFE composites, the C1s

spectrum can be fitted into subpeaks representing graphite (284.8 eV), $(C_2F_4)_n$ (292.25 eV), traces of organic compounds (286.41 eV), and metal carbonate (288.67 eV). The O1s spectrum indicated the presence of $(Al/Mg)Si_4O_{10}(OH)_2 \cdot nH_2O$ at the subpeak of 531.93 eV and SiO_2 at 533.40 eV. The Fe2p spectrum fitted into the subpeaks at 706.74 eV, 707.83 eV, and 709.55 eV indicated the presence of Fe, FeO, and Fe_3O_4 , respectively. The Mg1s spectrum can be fitted into the characteristic subpeak of MgO at 1302.94, $MgSiO_3$ at 1304.15 eV, Mg_2SiO_4 at 1305.11 eV, and $(Al/Mg)Si_4O_{10}(OH)_2 \cdot nH_2O$ at 1305.93 eV. The Si2p spectrum can be fitted into subpeaks located at 101.66 eV, 102.55 eV, and 103.55 eV, corresponding to $(Al/Mg)Si_4O_{10}(OH)_2 \cdot nH_2O$, $CaSiO_3$, and SiO_2 , respectively. The Ca2p spectrum can be fitted into the subpeaks of $CaSiO_3$ (347.55 eV), CaO (351.06 eV), and CaF_2 (352.58 eV). An XPS analysis was performed on the worn surfaces of the 10Atg/PTFE and 10Wl/PTFE composites. Mg_2SiO_4 , SiO_2 , and $MgSiO_3$ were observed on the worn 10Atg/PTFE composite surface, while SiO_2 and CaO were identified on the worn 10Wl/PTFE composite surface. Notably, except for the (10Atg + 20Wl)/PTFE composite, no iron-containing substances were found on the worn surface.

Wollastonite is a typical calcium metasilicate mineral composed mainly of $CaSiO_3$ and usually contains a small amount of free silica and calcium oxide impurities. The presence of impurities may be the main reason for the identification of CaO and SiO_2 in the XPS spectra of the unworn (10Atg + 20Wl)/PTFE composites, except for wollastonite and antigorite minerals. For the worn (10Atg + 20Wl)/PTFE composite surface, new compositions of MgO, Mg_2SiO_4 , $MgSiO_3$, Fe_3O_4 , FeO, and Fe were identified from the XPS spectra. Table 2 shows the relative content of silicon-containing compounds on the worn and unworn surfaces of the PTFE matrix composites, calculated by comparing the peak areas of the Si2p peak areas. After rubbing against the steel ball, the content of antigorite and/or wollastonite minerals decreased compared to that of the unworn surface, while the content of SiO_2 increased. In comparison, the increase in SiO_2 on the surface of the (10Atg + 20Wl)/PTFE composites was much higher than the sum of that of PTFE filled with mono antigorite (10Atg/PTFE composites) or wollastonite (10Wl/PTFE composites).

Table 2. Relative content of Si-containing compounds on worn and unworn composites surface.

Composites	Relative Content (wt.%)		
	Antigorite	Wollastonite	SiO_2
	Unworn/Worn	Unworn/Worn	Unworn/Worn
10Atg/PTFE	88.43/83.75	0.00/0.00	11.57/16.25
10Wl/PTFE	0.00/0.00	88.14/84.26	11.86/15.74
(10Atg + 20Wl)/PTFE	31.37/25.21	55.70/41.92	12.93/32.87

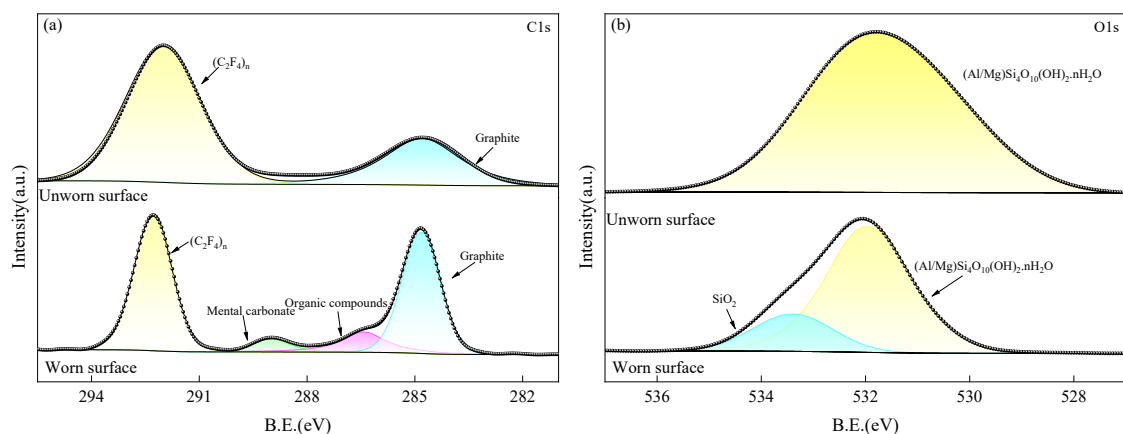


Figure 11. Cont.

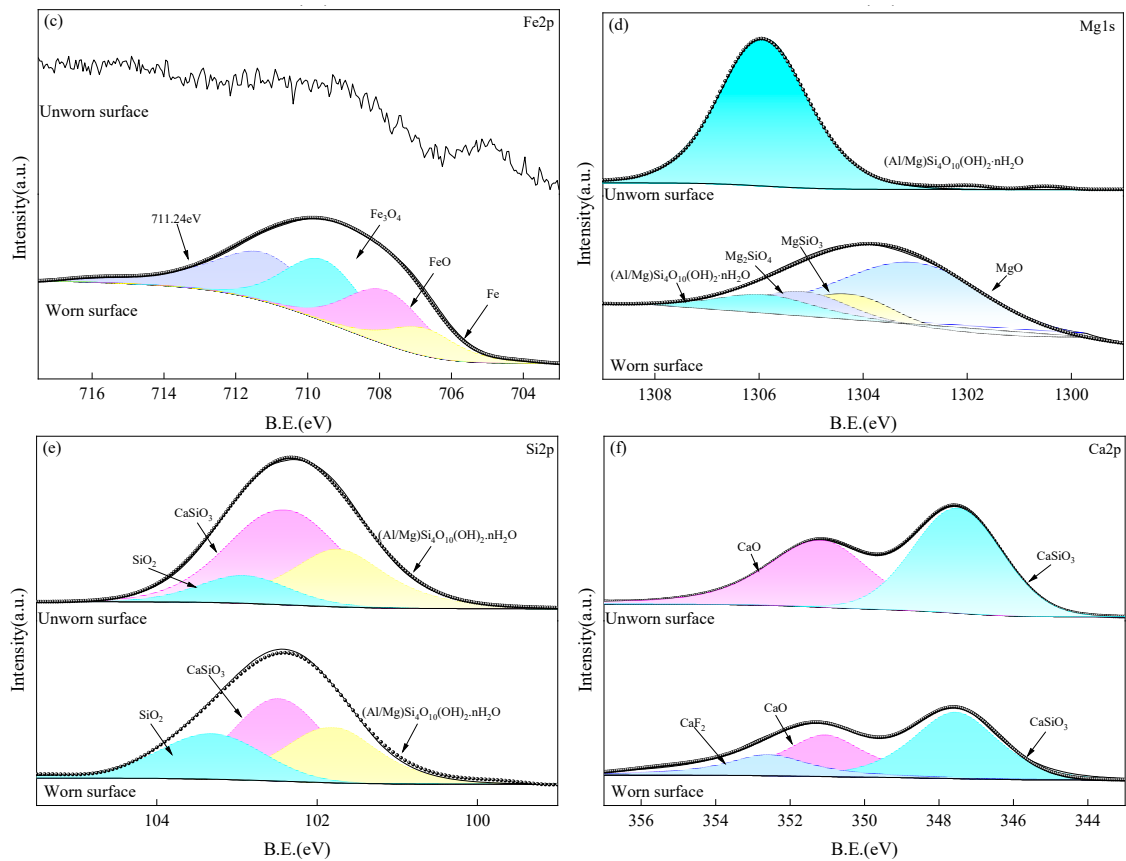
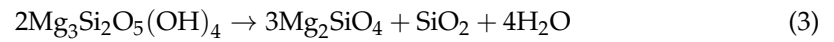
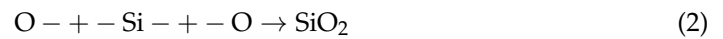


Figure 11. XPS spectra of (a) C1s, (b) O1s, (c) Fe2p, (d) Mg1s, (e) Si2p, and (f) Ca2p on the unworn and worn surfaces of (10Atg + 20WI)/PTFE composites.

Dehydration reactions under high-temperature and high-pressure conditions are among the most important characteristics of antigorite minerals [26]. During the friction process, the local flash temperature and high pressure can induce partial destruction or twisting of silica–oxygen tetrahedra and magnesia hydroxide octahedra in antigorite crystals as well as their dehydration reaction. Once the layer structure of the antigorite was partially destroyed, active atoms such as O, Si, and Mg were released, which could form MgO and SiO₂ through the reaction described by Equations (1) and (2) [27]. The dehydration reaction transforms antigorite into forsterite (Mg₂SiO₄), SiO₂, and enstatite (MgSiO₃), as expressed in Equations (3) and (4) [28]. In addition, wollastonite decomposes into SiO₂ and CaO at high temperatures according to Equation (5). The above chemical reactions occurred for a portion of the antigorite and wollastonite minerals in the (10Atg + 20WI)/PTFE composites during the friction and wear processes, resulting in the appearance of new phases of hard particles and an increase in SiO₂ content. This is undoubtedly beneficial for improving the wear resistance of the composites. Moreover, antigorite and wollastonite may have a synergistic effect during the friction process, which promotes both the dehydration reaction of antigorite and decomposition reaction of wollastonite, thereby transforming more minerals into hard phases such as Mg₂SiO₄, SiO₂, and MgSiO₃. This resulted in a significant increase in SiO₂ and a decrease in the mineral content on the worn surface of the (10Atg + 20WI)/PTFE composite material, as shown in Table 2. In addition, the presence of oxides and elemental phases of Fe on the worn surface also improves the tribological properties. It can be determined that Fe came from the counterpart GCr15 steel ball surface, which reacted with oxygen from the air or was released by antigorite. The presence of iron on the wear surface indicates an increase in the hardness of the biphasic mineral-reinforced composites and also verifies the corresponding Shore hardness. The composite material with high hardness in the process of grinding against the steel ball, the iron component on the surface of the steel ball is ground down and gradually transferred

to the wear surface of the composite material, and the iron element on the wear surface is affected by the high temperature generated by the friction process, and part of it undergoes a chemical reaction to generate iron oxides. Iron and iron oxide as a hard phase can also improve the wear resistance of the composite wear surface.



3.5. Worn Steel Surface Analysis

Figure 12 shows SEM images and EDS patterns of the worn surfaces of the GCr15 steel balls after rubbing against pure PTFE and the composites. The worn steel surface rubbing against pure PTFE was mainly composed of Fe, C, and O, and scratches along the sliding direction were evident. Owing to the good non-adhesion and low surface energy of PTFE, it is usually difficult for the C and F elements in the polymer to transfer to the surface of the counterpart steel balls during friction. Therefore, it was deduced that the C element on the worn ball surface originated from the GCr15 steel, whereas the presence of a small amount of O was the result of air oxidation during friction. For the worn steel surface rubbed against 10Atg/PTFE composites, newly appearing elements of Si, Mg, and F were found, and the O content was elevated, indicating that PTFE and antigorite have transferred or undergone tribochemical reactions. Based on the SEM morphology, a discontinuous film was generated on the worn surface. For the worn steel surface rubbed against the 10Wl/PTFE composites, Si, Ca, F, O, and C were observed. For the worn steel surface rubbed against the (10Atg + 20Wl)/PTFE composites, a new element, Ca, appeared based on the previous composition, while the O content was further increased, leading to the formation of a more continuous and denser film of transfer or tribochemical reactions.

XPS analysis was performed to determine the chemical composition of the surface film formed on the worn steel balls and further clarify whether it was a transfer film or a tribofilm. Figure 13 shows the XPS spectra of the main elements on the worn steel surface rubbing against the 10Atg/PTFE and (10Atg + 20Wl)/PTFE composites. For the worn surface rubbed against the 10Atg/PTFE composites, the C1s spectrum can be fitted as two subpeaks located at 284.8 eV and 285.42 eV, corresponding to graphite and pollution carbon, respectively. The O1s spectrum can be fitted into subpeaks representing metal oxides (530.13 eV), (Al/Mg)Si₄O₁₀(OH)₂·nH₂O (531.81 eV), and organic compounds (533.48 eV). The Fe2p spectrum can be fitted into subpeaks at 706.57 eV, 707.93 eV, 709.38 eV, and 710.90 eV, corresponding to Fe, FeO, Fe₃O₄, and Fe₂O₃, respectively. The Mg1s spectrum indicated the presence of MgO at 1303.2 eV, MgSiO₃ (enstatite) at 1304.15 eV, Mg₂SiO₄ (forsterite) at 1305.25 eV, and (Al/Mg)Si₄O₁₀(OH)₂·nH₂O (antigorite) at 1305.95 eV. The Si2p spectrum can be fitted into subpeaks of (Al/Mg)Si₄O₁₀(OH)₂·nH₂O at 101.85 eV, Mg₂SiO₄ at 103.25 eV, and MgSiO₃ at 105.12 eV. The results indicate that a tribofilm was formed on the worn steel surface.

For the worn steel surface rubbed against the (10Atg + 20Wl)/PTFE composites, the intensity of the spectra increased, and the positions of the fitted subpeaks and corresponding substances changed completely. The C1s spectrum can be fitted into subpeaks representing graphite (284.8 eV), polluted carbon (285.52 eV), organic matter (286.8 eV), and (C₂F₄)_n at 288.03 eV. The identification of (C₂F₄)_n indicates the transfer of PTFE from the composites to the steel ball surface. The O1s spectrum indicated the presence of antigorite at subpeak of 532.1 eV, organic compounds at 533.65 eV, and metal oxides at subpeaks of both 529.35 eV and 530.50 eV. The Fe2p spectrum can be fitted into the subpeaks at 707.75 eV, 709.92 eV, 712.10 eV, 715.68 eV, and 723.4 eV, corresponding to FeO, Fe_xO_y, Fe₂O₃, FeOOH, and Fe₃O₄,

respectively. The Mg1s spectrum can be fitted into the characteristic subpeak of MgO at 1303.23 eV, MgSiO₃ at 1304.34 eV, Mg₂SiO₄ at 1305.16 eV, and (Al/Mg)Si₄O₁₀(OH)₂·nH₂O at 1305.92 eV. The Si2p spectrum can be fitted into subpeaks of (Al/Mg)Si₄O₁₀(OH)₂·nH₂O at 101.59 eV, Mg₂SiO₄ at 103.14 eV, SiO₂ at 103.68 eV, and MgSiO₃ at 105.36 eV. It is noted that the newly emerged Ca2p spectrum can be fitted into subpeaks located at 352.77 eV and 349.55 eV, corresponding to CaF₂ and CaO, respectively. Moreover, no elemental iron was found, and all the Fe existed in the form of oxides or hydroxides, indicating a complete tribochemical reaction. Meanwhile, only small amounts of CaO and SiO₂ were found on the worn surface of the steel ball rubbed against the 10WI/PTFE composites according to the XPS analysis, which is not shown in Figure 13 because of space limitations.

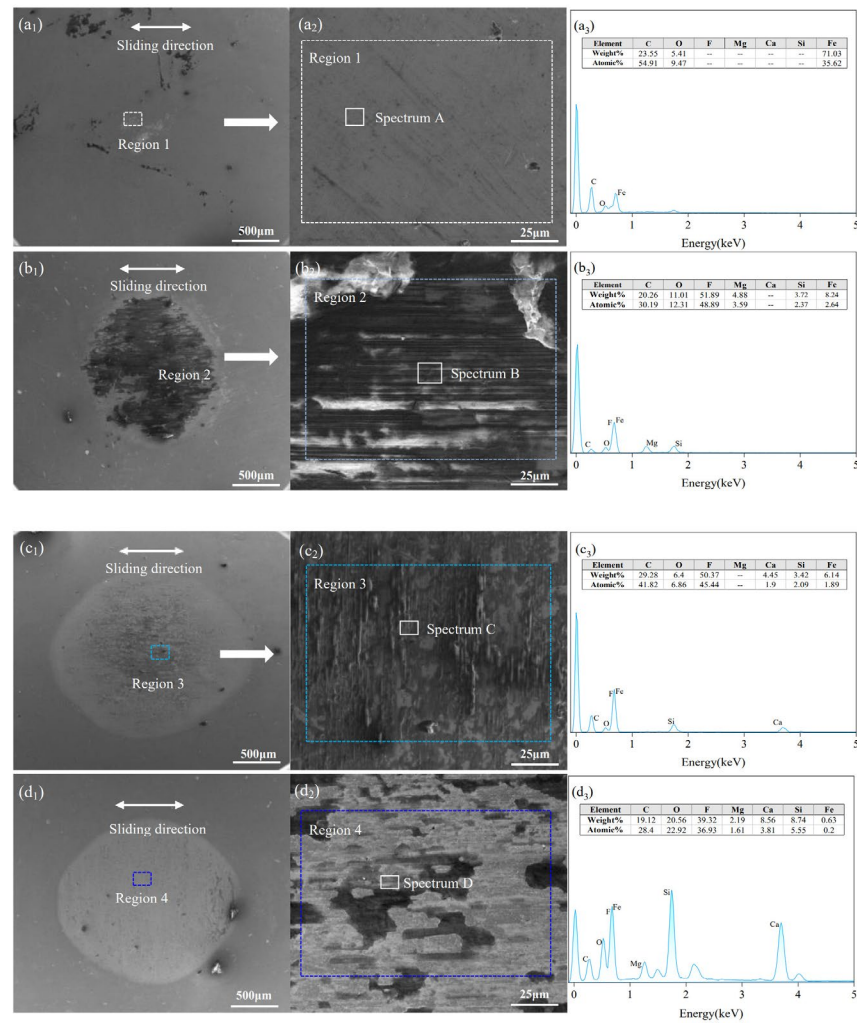


Figure 12. SEM images and EDS patterns of worn steel ball surface rubbed against (a₁–a₃) PTFE, (b₁–b₃) 10Atg/PTFE, (c₁–c₃) 10WI/PTFE, and (d₁–d₃) (10Atg + 20WI)/PTFE.

Table 3 shows the relative contents of Si-containing compounds on the worn surfaces of steel balls rubbed against different PTFE matrix composites, calculated by comparing the peak areas of the Si2p spectra. Similar to the XPS analysis results of the worn PTFE matrix composite surfaces, the MgSiO₃, Mg₂SiO₄, and SiO₂ contents on the worn surface rubbed against the (10Atg + 20WI)/PTFE composites were much higher than those against the 10Atg/PTFE composites, indicating a more thorough dehydration reaction process of antigorite and decomposition reaction of wollastonite. The above XPS analysis results further indicate a cooperative effect between wollastonite and antigorite minerals, which can promote the tribochemical reaction between antigorite wollastonite and the rubbing surfaces. Furthermore, a pure tribofilm was formed on the worn steel surface rubbed

against PTFE matrix composites filled with mono antigorite or wollastonite, whereas a tribofilm-containing PTFE transfer film was formed on the worn steel surface rubbed against composites filled with both antigorite and wollastonite.

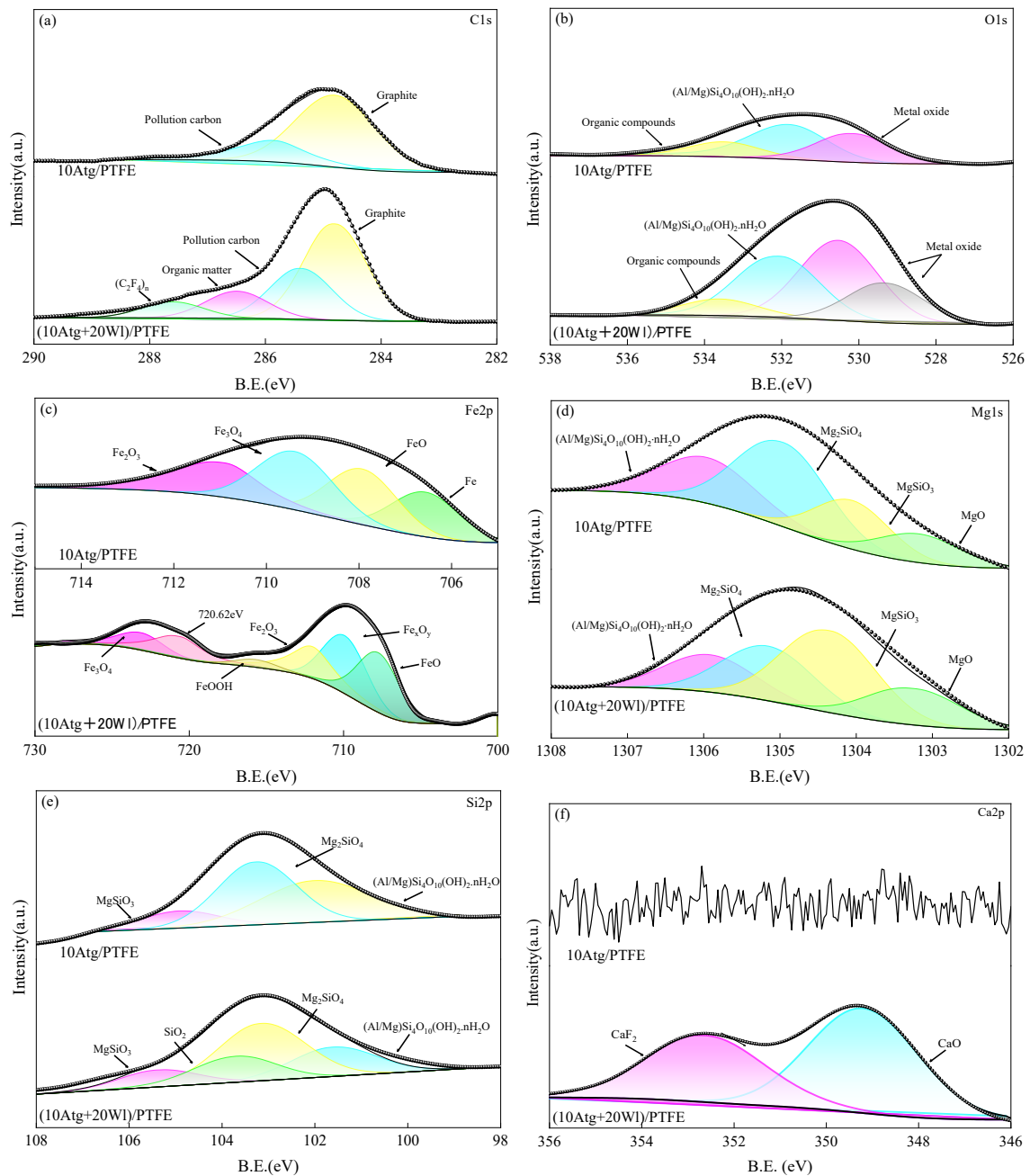


Figure 13. XPS spectra of (a) C1s, (b) O1s, (c) Fe2p, (d) Mg1s, (e) Si2p, and (f) Ca2p on the worn steel ball surface rubbed against 10Atg/PTFE and (10Atg + 20Wl)/PTFE.

Table 3. Relative content of Si-containing compounds on the worn steel ball surface rubbed against the 10Atg/PTFE and (10Atg + 20Wl)/PTFE composites.

Rubbed against	Relative Content of Silicon-Containing Compounds (wt.%)			
	Antigorite	MgSiO ₃	Mg ₂ SiO ₄	SiO ₂
10Atg/PTFE	44.41	9.75	41.78	4.06
(10Atg + 20Wl)/PTFE	22.71	12.16	45.30	19.83

To further investigate the microstructure of the tribofilm, a cross-sectional specimen for TEM analysis was prepared using a FIB/SEM system on the selected worn area of the steel ball rubbed against the (10Atg + 20Wl)/PTFE composites. Figure 14 shows the images of sampling location and cross-sectional morphology of the TEM specimen, as well as the TEM morphology and elemental distribution maps of the selected region. A continuous and compact tribofilm with a thickness of 400–500 nm was formed, which bonded well to the worn steel surface. This film is mainly composed of the characteristic elements of antigorite and wollastonite, such as Mg, Al, Ca, Si, and O, as well as C and F, which is consistent with the EDS analysis of the worn surface.

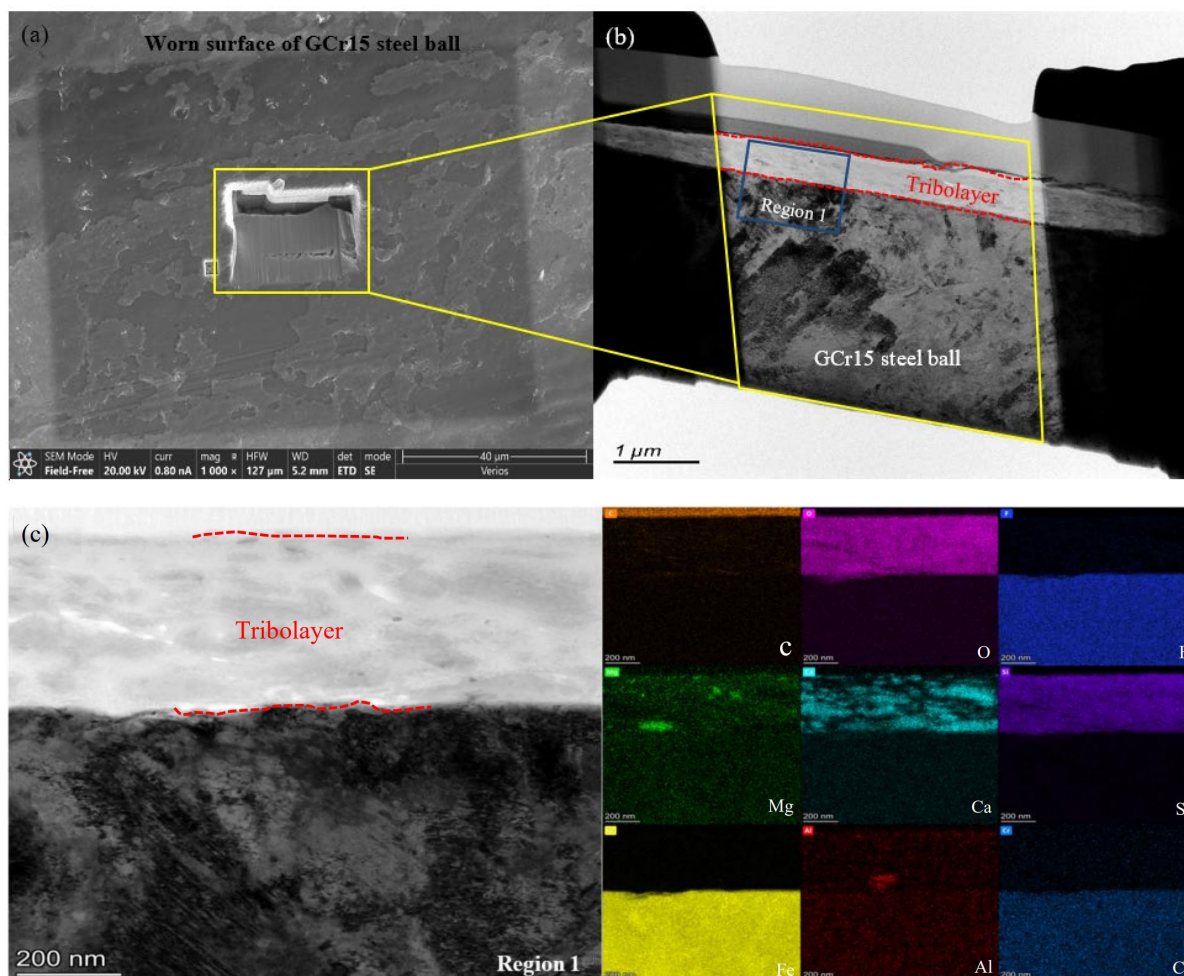


Figure 14. Images of (a) sampling location, (b) cross-sectional morphology of the TEM specimen, and (c) TEM morphology and elemental distribution maps of the selected region on the worn steel surface rubbed against the (10Atg + 20Wl)/PTFE composites.

Figure 15 shows HRTEM images and selected-area electron diffraction (SAED) patterns of the tribofilm formed on the worn steel surface. The majority of the film was a light-gray amorphous phase, which was confirmed as SiO_2 based on FFT analysis (Figure 15a). Within the amorphous SiO_2 matrix, many gray and dark-gray particulates are distributed with a clean and defect-free interface. The gray particles can be identified as Al_2O_3 , and the interplanar spacings of 0.657 and 0.797 nm in the HRTEM image correspond to the (101) and (010) planes, respectively (Figure 15b). Similarly, the dark-gray particles can be identified as three silicates, $\text{CaMg}(\text{SiO}_3)_2$, CaSiO_3 (wollastonite), and MgSiO_3 (enstatite), according to the HRTEM images and FFT analysis shown in Figure 15c–e. Notably, no phases such as CaF_2 , MgSiO_3 , Mg_2SiO_4 , CaO , or iron oxides identified in the XPS analysis were found in

the tribofilm. This may be due to the limited TEM analysis area caused by the small size of the TEM specimen or the lower content of these substances.

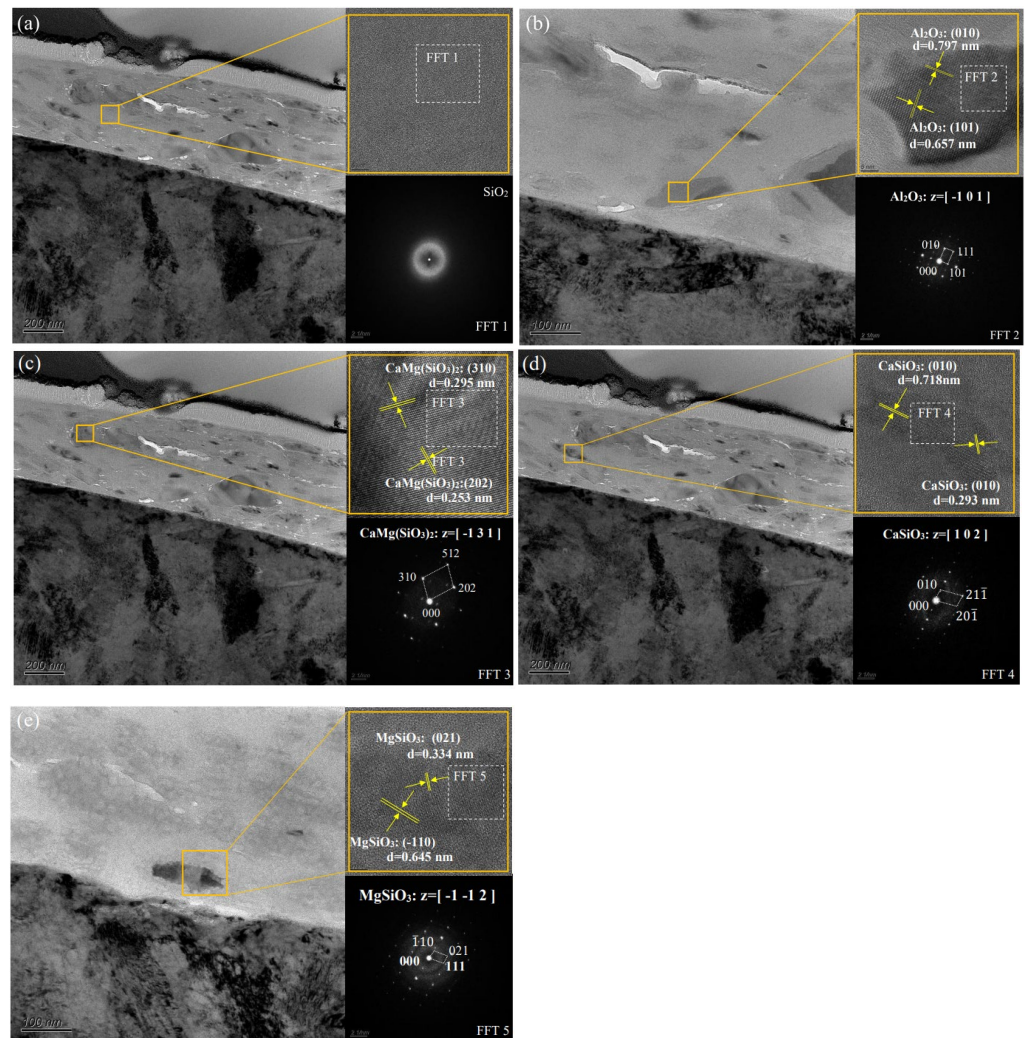


Figure 15. HRTEM morphology and SAED patterns of (a) SiO_2 , (b) Al_2O_3 , (c) $\text{CaMg}(\text{SiO}_3)_2$, (d) CaSiO_3 , and (e) MgSiO_3 in the tribofilm formed on the worn steel surface.

3.6. Tribological Mechanism

It is generally believed that the reduction in the friction coefficient and improvement in the wear resistance of PTFE matrix composites can be attributed to the improvement in the mechanical properties of the composites [29]. In this study, the Shore hardness of the composites was significantly increased by the filling of mono antigorite or wollastonite mineral powder into PTFE, which improved the anti-abrasive wear and anti-plastic deformation of PTFE to a certain extent, resulting in a significant increase in the wear resistance of the 10Atg/PTFE or 10Wl/PTFE composites. Antigorite has a higher hardness than PTFE, and when antigorite is filled with PTFE, the antigorite will play the role of hardness enhancement to improve the wear resistance of PTFE. And wollastonite special needle column structure will play the role of rigidity enhancement to improve the wear resistance of PTFE. With the simultaneous addition of antigorite and wollastonite, the hardness and wear resistance of the composites were further improved owing to the slip between the PTFE macromolecular chains during loading. However, as mentioned earlier, the addition of excess minerals can increase the number of bonding interfaces between the mineral and PTFE matrix, leading to an increase in the number of potential defects and crack sources within the composites. Therefore, the hardness and wear resistance of the dual-phase

mineral-reinforced composites show a trend of first increased and then decreased with increasing mineral content.

In addition to the strengthening effect of the mineral particles, the complex physical and chemical reactions at the friction interface are the main reasons for the significant improvement in the tribological properties of PTFE matrix composites filled with antigorite and/or wollastonite, according to the worn surface analysis results in the present work. Antigorite minerals are composed of Mg-O octahedral layers and Si-O tetrahedral layers in a 1:1 ratio, and their crystal structures contain many active atomic groups and unsaturated bonds, such as O-Si-O, Si-O-Si, O-H-O, OH-Mg-OH/O, and -OH [30,31]. According to previous studies on phyllosilicates as lubricant additives, the crystal structure of antigorite is partially destroyed during friction. Dehydration reactions, release of highly reactive oxygen-containing atoms or atomic groups, and a series of complex tribochemical reactions occur for antigorite minerals under local high-pressure and high-temperature conditions [31–33]. A hard tribofilm, composed of iron oxides, SiO₂, dehydration reaction products, etc., can be formed on the worn surface under the lubrication of oil-containing antigorite powder, which contributes to good tribological behavior [34,35].

Apparently, the above reaction also occurred during the rubbing process for the tribopairs of the GCr15 steel ball and PTFE matrix composites filled with antigorite and/or wollastonite. For PTFE matrix composites filled with mono antigorite (10Atg/PTFE sample), the reactions shown in Equations (1)–(4) occurred during friction and wear. The antigorite in the composites released reactive groups and dehydrated under the action of frictional–thermal coupling effects. The tribochemical reaction products of various components were rolled, spread, and transferred between the composites/steel ball contact surface, and a tribofilm composed of Mg₂SiO₄, SiO₂, and MgSiO₃ was formed on both the composites and steel ball surface. For the composites filled with mono wollastonite (10Wl/PTFE sample), the reaction shown in Equation (5) occurred, and a tribofilm composed of CaO and SiO₂ was formed on the tribopairs' surface. It is evident that the formation of these hard reaction products improved the wear resistance of the PTFE matrix composites to a certain degree.

Compared with the mono addition of antigorite or wollastonite, simultaneously filling PTFE with the two minerals not only further reduced the friction and wear of the composites but also promoted the formation of a dense and continuous tribofilm, with hard tribochemical reaction products such as Mg₂SiO₄, SiO₂, and MgSiO₃ on the worn surface. Moreover, new CaF₂ phases appear in the tribofilm. This indicates that the two minerals had a synergistic effect on the tribological properties of PTFE. Mg₂SiO₄, MgSiO₃, SiO₂, CaO, and iron oxides as hard phases can improve the wear resistance of the composites, and CaF₂ as a high-temperature lubricant can reduce the frictional resistance between the friction partners, which can further improve the tribological properties of the composites. To further explain the synergistic principle of antigorite and wollastonite minerals, a thermal analysis was conducted on raw powders with different compositions. Figure 16 shows the TG–DSC curves of the raw powders of the pure PTFE and PTFE matrix composites. For pure PTFE, a small endothermic peak appears at 351.4 °C without mass loss. It can be determined that the temperature corresponds to the melting point of PTFE. A large endothermic peak appears at 589.7 °C, and the mass loss reached 100%, indicating that PTFE was completely decomposed at this temperature [36]. For the composites, the glass transition temperature decreased slightly, which may be because the addition of the mineral powders weakened the intermolecular bonding force of PTFE and increased the molecular free volume [37]. Two obvious endothermic peaks appeared in the temperature ranges of 615–640 °C and 705–735 °C, corresponding to the loss of interlayer water and structural water from antigorite during the dehydration reaction process, respectively. Owing to the loss of structural water, the crystal structure of antigorite was destroyed and reorganized, generating new phases of forsterite (Mg₂SiO₄) and enstatite (MgSiO₃) [38]. In comparison, the addition of wollastonite reduced the phase transition temperature of antigorite by approximately 40–70 °C.

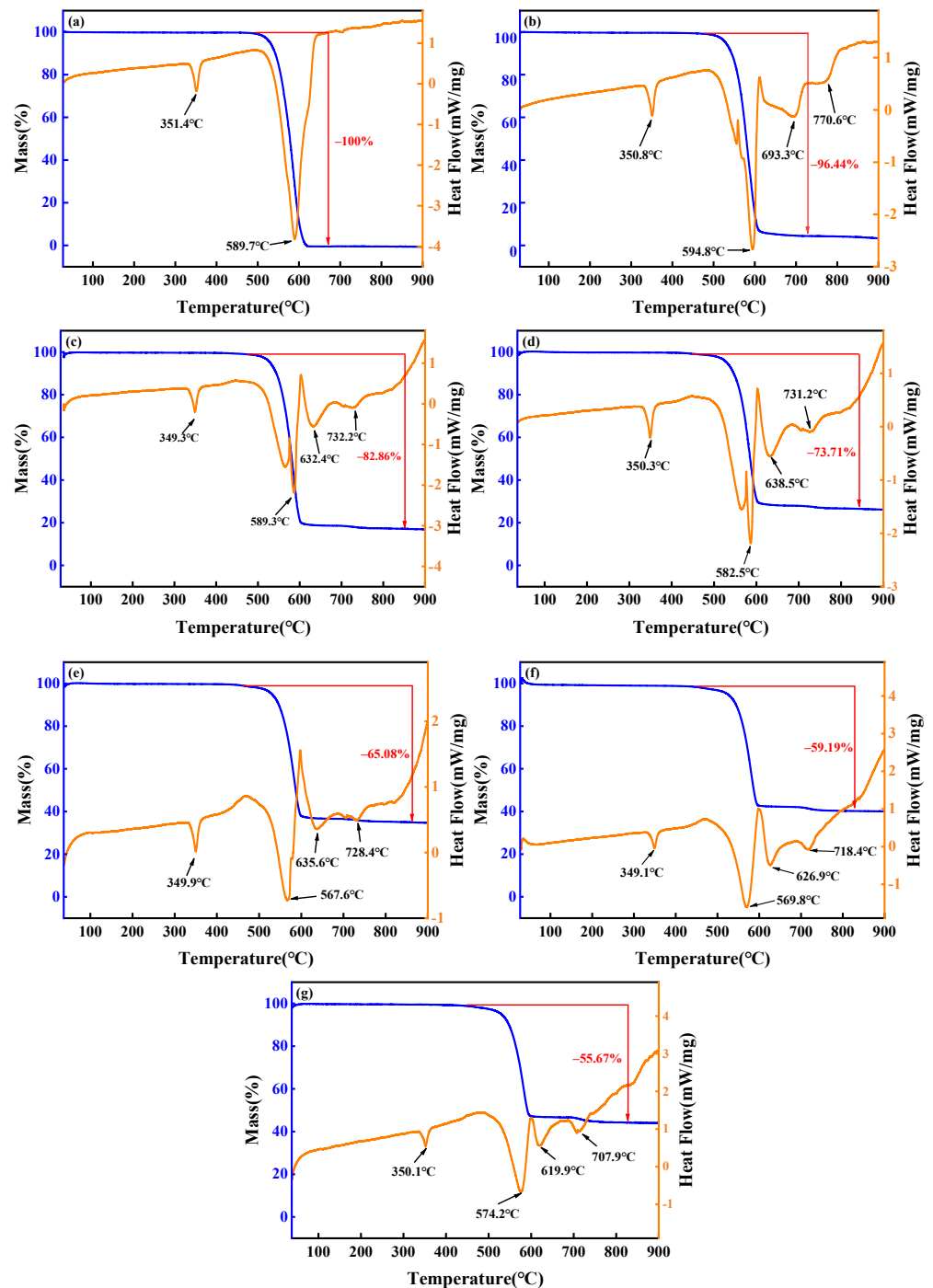
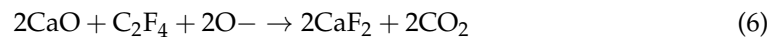


Figure 16. TG–DSC curves of raw powders of (a) PTFE, (b) 10Atg/PTFE, (c) (10Atg + 10Wl)/PTFE, (d) (10Atg + 20Wl)/PTFE, (e) (10Atg + 30Wl)/PTFE, (f) (15Atg + 20Wl)/PTFE, and (g) (20Atg + 20Wl)/PTFE.

Obviously, a reduction in the phase transition temperature is beneficial for accelerating the dehydration reaction and tribochemical reaction process of antigorite, as shown in Equations (1)–(4), under the thermal coupling effect during friction, thereby promoting the formation of a tribofilm and improving the tribological properties of composites. Under high-temperature conditions ranging from 400 to 450 °C, the PTFE molecular chains broke, leading to the decomposition of the polymer. This is mainly because of the high binding energy of the C-F bond in the PTFE molecular chains, which makes it relatively unstable at high temperatures, generating highly reactive fluoride gas and reacting with CaO released

by CaSiO_3 under the synergistic effect between the two minerals [39]. The possible reaction process is expressed by Equation (6).



Overall, the tribofilm was mainly composed of SiO_2 , MgSiO_3 , Mg_2SiO_4 , MgO , CaO , and CaF_2 , which were formed on the worn surfaces of both the antigorite/wollastonite mineral dual-phase-reinforced PTFE composites and their counterpart steel balls during friction and wear. First, the tribochemical reaction products of the hard phases, such as SiO_2 , MgSiO_3 , and Mg_2SiO_4 , undoubtedly improve the hardness of the worn surface based on the hardening effect of wollastonite and antigorite on PTFE. Second, CaF_2 , MgO , and CaO have good thin-film lubrication, thermal stability, and high-pressure resistance and are commonly used as high-performance solid lubricants and high-temperature friction-reducing additives [40]. They can continuously provide good lubrication at high temperatures and pressures in the friction contact microregion, thus further reducing the friction and wear of the composites. Finally, a tribofilm was formed on both tribopair surfaces, which transformed the friction between the original steel ball and composites into friction between the films, thereby protecting the “substrate” below the film. Moreover, complete iron oxides and $(\text{C}_2\text{F}_4)_n$ were only found on the worn surfaces of the dual-phase-reinforced PTFE composites and counterpart steel balls, respectively. This was also the result of the synergistic effect between antigorite and wollastonite, which promoted the oxidation of iron-based wear debris and the transfer of PTFE.

4. Conclusions

(1) Antigorite and wollastonite mineral dual-phase-reinforced PTFE matrix composites were prepared by filling PTFE with mineral powders through ball-milling, cold-pressing, and pressureless sintering methods. The composites have a dense structure and uniform distribution of mineral phases, with a Shore hardness increase of 18.7–23.7% compared to pure PTFE.

(2) Compared with mono antigorite or wollastonite minerals, PTFE matrix composites prepared by simultaneously filling the two minerals exhibited excellent tribological properties. The average friction coefficient and wear volume of the (10Atg + 20Wl)/PTFE composites were reduced by 44.2% and 71.4%, respectively, compared to those of pure PTFE, demonstrating optimal tribological performance.

(3) The reduction in friction and wear of the dual-phase-reinforced PTFE matrix composites is attributed to the reinforcement of the minerals as well as the complex physical and chemical reactions at the friction interface under the synergistic effects between the two minerals. A dense and continuous tribofilm mainly composed of SiO_2 , MgSiO_3 , Mg_2SiO_4 , MgO , CaO , $\text{CaMg}(\text{SiO}_3)_2$, and CaF_2 was formed on the worn surfaces of both the dual-phase-reinforced PTFE matrix composites and the counterpart steel ball during friction and wear, which contributed to the excellent tribological behaviors of the composites.

Author Contributions: Conceptualization, H.Y.; methodology, H.Y. and C.W.; project administration, H.Y.; validation, H.W., S.W. and Z.Y.; formal analysis, S.W. and Z.Y.; investigation, C.W. and H.W.; resources, Z.S.; formal analysis, H.W. and Z.S.; writing—original draft preparation, C.W. and Y.Y.; writing—review and editing, H.Y., Y.Y., Z.S. and Z.B.; visualization, X.Z.; supervision, Z.B.; project administration, H.Y.; All authors have read and agreed to the published version of the manuscript.

Funding: This research was funded by the National Natural Science Foundation of China grant number 52075544.

Data Availability Statement: Data are contained within the article.

Acknowledgments: The authors would like to acknowledge financial support from the National Natural Science Foundation of China (grant number 52075544).

Conflicts of Interest: The authors declare no conflict of interest.

References

1. Li, S.; Duan, C.; Li, X.; Shao, M.; Qu, C.; Zhang, D.; Wang, Q.; Wang, T.; Zhang, X. The effect of different layered materials on the tribological properties of PTFE composites. *Friction* **2020**, *8*, 542–552. [[CrossRef](#)]
2. Muraki, M.; Nakamura, K.; Nakatsu, K. Effect of PTFE and some additives of engine oil on tribological properties between polyamide and carbon steel. *Tribol. Online* **2018**, *13*, 67–74. [[CrossRef](#)]
3. Samyn, P. Tribological properties and thermomechanical analysis of unsaturated polyester fabric composite in oscillating line-contact sliding. *Tribol. Int.* **2016**, *99*, 127–139. [[CrossRef](#)]
4. Yan, Y.; Yang, C.; Dong, W.; Yan, P.; Wang, P.; Yan, X.; Jia, Z. Effect of nano-serpentine and nano-La₂O₃ on the frictional properties of PTFE composites in seawater environment. *Ind. Lubr. Tribol.* **2023**, *75*, 380–386. [[CrossRef](#)]
5. Hunke, H.; Soin, N.; Gebhard, A.; Shah, T.; Kramer, E.; Witan, K.; Narasimulu, A.A.; Siores, E. Plasma modified Polytetrafluoroethylene (PTFE) lubrication of α -olefin-copolymer impact-modified Polyamide 66. *Wear* **2015**, *338–339*, 122–132. [[CrossRef](#)]
6. Shi, Y.; Feng, X.; Wang, H.; Lu, X. The effect of surface modification on the friction and wear behavior of carbon nanofiber-filled PTFE composites. *Wear* **2008**, *264*, 934–939. [[CrossRef](#)]
7. Gheisari, R.; Polycarpou, A.A. Tribological performance of graphite-filled polyimide and PTFE composites in oil-lubricated three-body abrasive conditions. *Wear* **2019**, *436*, 203044. [[CrossRef](#)]
8. Johansson, P.; Marklund, P.; Björling, M.; Shi, Y.J. Effect of humidity and counterface material on the friction and wear of carbon fiber reinforced PTFE composites. *Tribol. Int.* **2021**, *157*, 106869. [[CrossRef](#)]
9. Wu, C.; Wu, Y.; Zhao, H.; Li, S.; Ni, J.; Li, X. Influence of hardness of nanoparticle additive in PTFE solid lubricant on tribological properties of GCr15 steel with bionic texture. *Tribol. Int.* **2023**, *189*, 108915. [[CrossRef](#)]
10. Yin, Y.L.; Yu, H.L.; Wang, H.M.; Zhou, X.Y.; Song, Z.Y.; Xu, Y.; Xu, B.S. Tribological performance of phyllosilicate minerals as lubricating oil additives. *J. Chin. Ceram. Soc.* **2020**, *48*, 299–308. [[CrossRef](#)]
11. Qin, Y.; Wu, M.; Yang, Y.; Yang, Y.; Yang, G. Enhanced ability of halloysite nanotubes to form multilayer nanocrystalline tribofilms by thermal activation. *Tribol. Int.* **2022**, *174*, 107718. [[CrossRef](#)]
12. Zhang, Z.; Yin, Y.L.; Yu, H.L.; Wang, H.M.; Song, Z.Y.; Zhou, X.Y.; Ji, X.C.; Zhang, W.; Xu, B.S. Tribological behaviors and mechanisms of surface-modified sepiolite powders as lubricating oil additives. *Tribol. Int.* **2022**, *173*, 107637. [[CrossRef](#)]
13. Sleptsova, S.A.; Kapitonova, Y.V.; Lazareva, N.N.; Makarov, M.M. Wear-resistant polymer composites based on polytetrafluoroethylene and layered silicates. *Russ. Mater. Sci.* **2016**, *2016*, 149–154. [[CrossRef](#)]
14. Bai, Z.; Yang, N.; Guo, M.; Li, S. Antigorite: Mineralogical characterization and friction performances. *Tribol. Int.* **2016**, *101*, 115–121. [[CrossRef](#)]
15. Jia, Z.; Yang, Y.; Chen, J.; Yu, X. Influence of serpentine content on tribological behaviors of PTFE/serpentine composite under dry sliding condition. *Wear* **2010**, *268*, 996–1001. [[CrossRef](#)]
16. Meng, Z.; Wang, Y.; Xin, X.; Liu, H.; Yan, Y.; Yan, F. Effects of attapulgite on the worn surface and fretting wear resistance property of UHMWPE composites. *Ind. Lubr. Tribol.* **2020**, *72*, 821–827. [[CrossRef](#)]
17. Lai, S.Q.; Li, T.S.; Liu, X.J.; Lv, R.G. A study on the friction and wear behavior of PTFE filled with acid treated nano-attapulgite. *Macromol. Mater. Eng.* **2004**, *289*, 916–922. [[CrossRef](#)]
18. Tarasova, P.N.; Danilova, S.N.; Okhlopkova, A.A.; Lazareva, N.N. The Influence of mechanically activated kaolinite and magnesium spinel on tribological properties and structure of PTFE friction surfaces. *J. Frict. Wear* **2022**, *43*, 312–317. [[CrossRef](#)]
19. Liu, Y.; Wang, S.; Liu, H.; Liu, W.; He, S.; Zhu, C. Tribological properties of Nylon1010/Wollastonite composites. *Eng. Plast. Appl.* **2018**, *46*, 5–8. [[CrossRef](#)]
20. Wu, D.; Bai, Z.; Zhang, J. Friction and Wear Properties, Mechanism of attapulgite-wollastonite/PTFE composites. *J. Chin. Ceram. Soc.* **2021**, *49*, 2078–2088. [[CrossRef](#)]
21. Levenstein, M.A.; Anduix-Canto, C.; Kim, Y.Y.; Holden, M.A.; González Niño, C.; Green, D.C.; Foster, S.E.; Kulak, A.N.; Govada, L.; Chayen, N.E.; et al. Droplet microfluidics XRD identifies effective nucleating agents for calcium carbonate. *Adv. Funct. Mater.* **2019**, *29*, 1808172. [[CrossRef](#)]
22. Kim, H.B.; Han, B.; Lee, M.H. Enhanced filtration characteristics of a PTFE foam-coated filter using PTFE nanofibers. *Mater. Chem. Phys.* **2023**, *305*, 127970. [[CrossRef](#)]
23. Benk, A. The affects of heat and/or acid treatment on bleaching properties of serpentine to be utilized in reclaiming waste engine oil. *Fuel* **2021**, *290*, 120022. [[CrossRef](#)]
24. Ribas, R.G.; Campos, T.M.B.; Schatkoski, V.M.; de Menezes, B.R.C.; Montanheiro, T.L.D.; Thim, G.P. α -wollastonite crystallization at low temperature. *Ceram. Int.* **2020**, *46*, 6575–6580. [[CrossRef](#)]
25. Yang, D.; Wang, Y.; Dong, Y.; Gong, J.; Gao, G.; Wang, H. Tribological performance of different nanoparticles reinforced PPS-PTFE blends. *J. Funct. Mater.* **2014**, *45*, 6011–6015. [[CrossRef](#)]
26. Lafay, R.; Baumgartner, L.P.; Delacour, A. Preservation of mantle heterogeneities and serpentinization signature during antigorite dehydration: The example of the Bergell contact aureole. *J. Metamorph. Geol.* **2023**, *41*, 377–399. [[CrossRef](#)]
27. Zhang, B.; Xu, B.; Xu, Y.; Wu, Y.; Zhang, B. Friction reduction and anti-wear mechanism of serpentine micro powders for spheroidal graphite iron tribopair. *J. Chin. Silic. Soc.* **2009**, *37*, 2037–2042. [[CrossRef](#)]
28. Wang, Y.; Wei, Y.; Peng, B.; Li, B.; Zhou, S. Thermal decomposition of high-magnesium low-nickel laterite: Theoretical calculation and experimental study. *Mater. Rev.* **2019**, *33*, 1406–1411. [[CrossRef](#)]

29. Erdemir, A.; Ramirez, G.; Eryilmaz, O.L.; Narayanan, B.; Liao, Y.; Kamath, G.; Sankaranarayanan, S.K. Carbon-based tribofilms from lubricating oils. *Nature* **2016**, *536*, 67–71. [[CrossRef](#)]
30. Zulumyan, N.; Isahakyan, A.; Beglaryan, H.; Melikyan, S. A study of thermal decomposition of antigorite from dunite and lizardite from peridotite. *J. Therm. Anal. Calorim.* **2018**, *131*, 1201–1211. [[CrossRef](#)]
31. Wu, J.; Wang, X.; Zhou, L.; Wei, X.; Wang, W. Formation factors of the surface layer generated from serpentine as lubricant additive and composite reinforcement. *Tribol. Lett.* **2017**, *65*, 93–99. [[CrossRef](#)]
32. Yu, H.; Xu, Y.; Shi, P.; Wang, H.; Zhang, W.; Xu, B. Effect of thermal activation on the tribological behaviours of serpentine ultrafine powders as an additive in liquid paraffin. *Tribol. Int.* **2011**, *44*, 1736–1741. [[CrossRef](#)]
33. Zhang, B.; Xu, Y.; Gao, F.; Shi, P.; Xu, B.; Wu, Y. Sliding friction and wear behaviors of surface-coated natural serpentine mineral powders as lubricant additive. *Appl. Surf. Sci.* **2010**, *257*, 2540–2549. [[CrossRef](#)]
34. Li, G.; Bai, Z.; Zhao, P. Antifriction repair function of serpentine on Fe based metal friction pairs. *J. Chin. Ceram. Soc.* **2018**, *46*, 306–314. [[CrossRef](#)]
35. Qi, X.; Jia, Z.; Yang, Y.; Fan, B. Characterization and auto-restoration mechanism of nanoscale serpentine powder as lubricating oil additive under high temperature. *Tribol. Int.* **2011**, *44*, 805–810. [[CrossRef](#)]
36. Odochian, L.; Moldoveanu, C.; Carja, G. Contributions to the thermal degradation mechanism under air atmosphere of PTFE by TG–FTIR analysis: Influence of the additive nature. *Thermochim. Acta* **2013**, *558*, 22–28. [[CrossRef](#)]
37. Zhang, F.; Du, C.; Zhang, Y. Dynamic mechanical thermal analysis of PP/POE/Nano-meter CaCO₃. *Chin. Plast. Ind.* **2005**, *33*, 19–22. [[CrossRef](#)]
38. Zheng, W.; Zhang, Z.; Zhao, F.; Xu, D. Heat treating serpentine powder and its effect on the tribological of lube base oil. *Pet. Process. Petrochem.* **2013**, *44*, 71–74. [[CrossRef](#)]
39. Ma, L.; Jia, W.; Hou, K.; Yang, Y.; Li, Z.; Yang, S.; Wang, J. Similar chemical composition with different tribological properties: Influences of C-F bond strength and carbon-skeleton structure on fluorinated graphene and PTFE. *Tribol. Int.* **2022**, *165*, 107250. [[CrossRef](#)]
40. Makhesana, M.A.; Patel, K.M. Improvement in friction and wear characteristics using CaF₂ as a solid lubricant at different conditions. *Met. Powder Rep.* **2020**, *76*, S55–S65. [[CrossRef](#)]

Disclaimer/Publisher’s Note: The statements, opinions and data contained in all publications are solely those of the individual author(s) and contributor(s) and not of MDPI and/or the editor(s). MDPI and/or the editor(s) disclaim responsibility for any injury to people or property resulting from any ideas, methods, instructions or products referred to in the content.